Vacuum magnetic linear birefringence using pulsed fields: the BMV experiment

Agathe Cadène, Paul Berceau, M. Fouché, Rémy Battesti, Carlo Rizzo

EPJ manuscript No.
(will be inserted by the editor)

Vacuum magnetic linear birefringence using pulsed fields

Status of the BMV experiment

A. Cadène, P. Berceau, M. Fouché, R. Battesti and C. Rizzo

Laboratoire National des Champs Magnétiques Intenses (UPR 3228, CNRS-UPS-UJF-INSA), F-31400 Toulouse Cedex, France, EU

Received : date / Revised version : date

Résumé We present the current status of the BMV experiment. Our apparatus is based on an up-to-date resonant optical cavity coupled to a transverse magnetic field. We detail our data acquisition and analysis procedure which takes into account the symmetry properties of the raw data with respect to the orientation of the magnetic field and the sign of the cavity birefringence. The measurement result of the vacuum magnetic linear birefringence $k_{\rm CM}$ presented in this paper was obtained with about 200 magnetic pulses and a maximum field of 6.5 T, giving a noise floor of about $8 \times 10^{-21}\,\mathrm{T}^{-2}$ at 3σ confidence level.

PACS. 12.20.Fv Experimental tests – 78.20.Ls Magneto-optical effects – 42.25.Lc Birefringence

1 Introduction

It is known since the beginning of the 20$^{\rm th}$ century that any medium shows a linear birefringence in the presence of a transverse external magnetic field $\boldsymbol{B}$. This effect is usually known as the Cotton-Mouton (CM) effect (see Ref. [1] and references therein). The existence of such a magnetic linear birefringence has also been predicted in vacuum around 1970 in the framework of Quantum ElectroDynamics (QED) [2,3]. It is one of the non-linear optical effects described by the Heisenberg-Euler effective lagrangian (see Ref. [4] and references therein) and it can be seen as the result of the interaction of the external magnetic field with quantum vacuum fluctuations. In a vacuum therefore the index of refraction $n_{\parallel}$ for light polarized parallel to $\boldsymbol{B}$ is expected to be different from the index of refraction $n_{\perp}$ for light polarized perpendicular to $\boldsymbol{B}$ such that [4] :

$$\Delta n_{\rm CM} = n_{\parallel} - n_{\perp}, \tag{1}$$

$$= k_{\rm CM} B^2. \tag{2}$$

At the first order in the fine structure constant α, $k_{\rm CM}$ can be written as :

$$k_{\rm CM} = 2\alpha^2\hbar^3/15\mu_0 m_{\rm e}^4 c^5, \tag{3}$$

with $\hbar$ the Planck constant over 2π, $m_{\rm e}$ the electron mass, c the speed of light in vacuum, and μ_0 the magnetic constant. Using the CODATA recommended values for fundamental constants [5], one obtains :

$$k_{\rm CM} \sim 4.0 \times 10^{-24}\mathrm{T}^{-2}. \tag{4}$$

In spite of several experimental attempts, the experimental proof of such a very fundamental QED prediction is still lacking [4]. All recent experiments, both completed or running, measure $\Delta n_{\rm CM}$ via the ellipticity ψ induced on a linearly polarized light propagating in the birefringent vacuum :

$$\psi = \pi k_{\rm CM} \frac{L_B}{\lambda} B^2 \sin 2\theta_{\rm P}, \tag{5}$$

where λ is the light wavelength, L_B is the path length in the magnetic field, and $\theta_{\rm P} = 45^\circ$ is the angle between the light polarization and the birefringence axis. This equation clearly shows that the critical experimental parameter is the product $B^2 L_B$. In order to increase the ellipticity to be measured, one usually uses an optical cavity to store light in the magnetic field region as long as possible. The total acquired ellipticity Ψ is linked to the ellipticity ψ acquired in the absence of cavity and depends on the cavity finesse F as :

$$\Psi = \frac{2F}{\pi}\,\psi. \tag{6}$$

After the theoretical calculations in the 70s, a first measurement of the $k_{\rm CM}$ value was published by the BFRT collaboration [6]. It was based on a superconducting magnet providing a maximum field of 3.9 T, and a multipass optical cavity. Spurious signals were always present (see Table V(b) in [6]). Final results gave $k_{\rm CM} = (2.2 \pm 0.8) \times 10^{-19}\,\mathrm{T}^{-2}$ at 3σ confidence level for 34 refections inside the cavity, and $k_{\rm CM} = (3.2 \pm 1.3) \times 10^{-19}\,\mathrm{T}^{-2}$ for 578 reflections. In 2008 a new measurement was published by the PVLAS collaboration using a Fabry-Pérot optical cavity and a superconducting magnet providing a 2.3 T field : $k_{\rm CM} = (1.4 \pm 2.4) \times 10^{-20}\ \mathrm{T}^{-2}$ at 3σ [7]. The same experiment at 5 T gave $k_{\rm CM} = (2.7 \pm 1.2) \times 10^{-20}\,\mathrm{T}^{-2}$ at

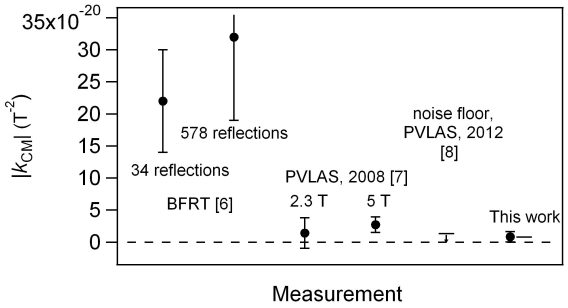

Figure 1. Comparison of reported absolute values of the vacuum magnetic linear birefringence and their uncertainties represented at 3σ.

3σ. More recently a new version of the PVLAS apparatus based on two 2.5 T permanent magnets and a Fabry-Pérot optical cavity reached a noise floor corresponding to $k_{\rm CM} = 1.3 \times 10^{-20}\,{\rm T}^{-2}$ at 3σ, but "only when no spurious signal was observed" [8]. All over our paper, we give error bars at 3σ corresponding to a confidence level of 99.8%, that usually indicates an evidence for a non-zero signal. All these measurements are summarized in Fig. 1. This clearly shows that vacuum CM measurements are true experimental challenges and that one has to focus not only on getting the best optical sensitivity and maximizing the signal to be measured, but also on minimizing all the unwanted systematic effects by decoupling the apparatus from their sources and by performing an appropriate data analysis.

In this paper we present a measurement of $k_{\rm CM}$ obtained using the first generation setup of the BMV *(Biréfringence Magnétique du Vide)* experiment at the National High Magnetic Field Laboratory of Toulouse, France - (LNCMI-T) [9]. The novelty of this experiment is the use of pulsed magnetic fields. This method allows to provide the highest magnetic fields in terrestrial laboratories without destroying the coil itself [4]. Our apparatus is also based on the use of an infrared Fabry-Pérot cavity among the sharpest in the world [10]. We calibrated our experiment using nitrogen gas [10], and recently published a high precision measurement of the Cotton-Mouton effect of helium gas compatible with the theoretical prediction [11]. We present our data acquisition and analysis procedure that takes into account the symmetry properties of the raw data with respect to the orientation of the magnetic field and the sign of the cavity birefringence. The measurement result of the vacuum magnetic linear birefringence $k_{\rm CM}$ presented in this paper was obtained with about 200 magnetic pulses and a maximum field of 6.5 T. It corresponds to the best noise floor ever reached. It is therefore a clear validation of our innovative experimental method.

2 Experimental setup

2.1 Apparatus

Our experimental setup is described in Refs. [11]. As shown in Fig. 2, 30 mW of a linearly polarized Nd :YAG laser beam ($\lambda = 1064$ nm) goes through an acousto-optic modulator (AOM) used in double pass for an adjustment of the laser frequency. It is then injected into a monomode optical fiber before entering a high finesse Fabry-Pérot cavity of length $L_{\rm c} = 2.27\,{\rm m}$, consisting of the mirrors M_1 and M_2. This corresponds to a cavity free spectral range of $\Delta^{\rm FSR} = c/2L_{\rm c} = 65.996\,{\rm MHz}$. The laser passes through an electro-optic modulator (EOM) creating sidebands at 10 MHz. We analyze the beam reflected by the cavity on the photodiode Ph_r. This signal is used to lock the laser frequency to the cavity resonance frequency using the Pound-Drever-Hall method [12], via the acousto-optic modulator and the piezoelectric and Peltier elements of the laser.

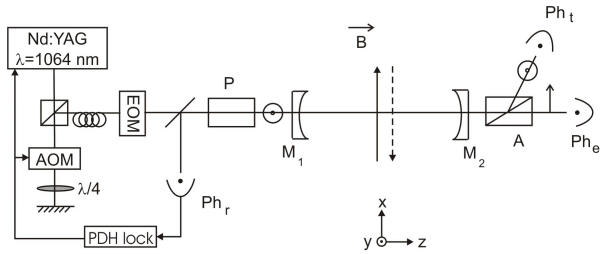

Figure 2. Experimental setup. EOM, electro-optic modulator; AOM, acousto-optic modulator; PDH, Pound-Drever-Hall; Ph, photodiode; P, polarizer; A, analyzer. See text for more details.

To measure the ellipticity induced by the Cotton-Mouton effect one needs a transverse magnetic field as high as possible. This is fulfilled using pulsed fields delivered by one magnet, named X-coil, especially designed in our laboratory. The principle of this magnet and its properties are described in details in Refs. [9,13]. It can provide a maximum field of more than 14 T over an equivalent length L_B of 0.137 m [10]. Data have been taken with a maximum magnetic field of 6.5 T reached within 1.70 ms while the total duration of a pulse is less than 10 ms as shown in Fig. 3. Moreover, we can remotely switch the high-voltage connections to reverse $\boldsymbol{B}$ in order to set it parallel or antiparallel to the x direction. The maximum repetition rate is 6 pulses per hour.

We infer the cavity finesse from the measurement of the photon lifetime τ [10]. Its value is regularly checked during data taking and we get $\tau = 1.07\,{\rm ms}$. The corresponding finesse is :

$$F = \frac{\pi c \tau}{L_{\rm c}}, \tag{7}$$

We get $F = 445\,000$ with a relative variation that does not exceed 6 % at the 3σ confidence level. This corresponds to a cavity linewidth $\Delta\nu = c/2FL_{\rm c}$ of 148 Hz. This is one of the sharpest infrared cavity in the world [10].

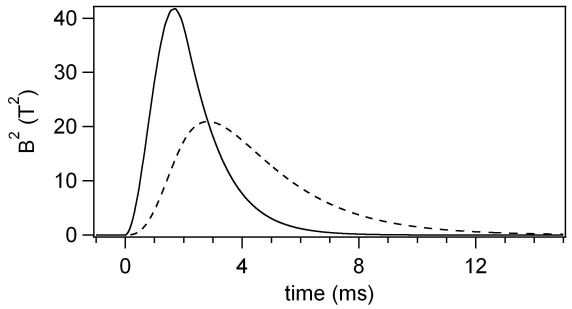

Figure 3. Square of the magnetic field amplitude as a function of time for a maximum field of 6.5 T. Solid black curve, B^2 ; dashed curve, $B_{\rm f}^2$.

Before entering the Fabry-Pérot cavity, light is polarized by the polarizer P. The beam transmitted by the cavity is then analyzed by the analyzer A crossed at maximum extinction. We extract both polarizations : parallel and perpendicular to P. The extraordinary ray, whose polarization is perpendicular to the incident polarization, is detected by the photodiode $\rm Ph_e$ (power $I_{\rm e}$), while the ordinary ray, whose polarization is parallel to the incident polarization, is detected by $\rm Ph_t$ (power $I_{\rm t}$).

All the optical devices from the polarizer to the analyzer are placed in an ultrahigh-vacuum chamber. During operation, the pressure inside the UHV vessel was about 10^{-7} mbar. We have monitored the vacuum quality with a residual gas analyzer. Residual gases can cause a measurable CM effect. Most important contributions come from N_2 and O_2 leading to a $k_{\rm CM}$ of $1.5\times10^{-23}\,\rm T^{-2}$. Moreover dielectric mirrors also induce a CM effect corresponding to an ellipticity of $8\times10^{-10}\,\rm rad.T^{-2}$ per reflection, as reported in Ref. [18]. The stray transverse magnetic field at the mirror position is smaller than $150\,\mu$T, giving in our case $k_{\rm CM}<1\times10^{-24}\,\rm T^{-2}$. We expect these CM effects to be smaller than the measured noise floor.

2.2 Signals

The ellipticity $\Psi(t)$ induced by the transverse magnetic field is related to the ratio of the extraordinary and ordinary powers as follows :

$$\begin{aligned}\frac{I_{\rm e}(t)}{I_{\rm t,f}(t)} &= \sigma^2+[\Gamma+\Psi(t)]^2,\\ &\simeq \sigma^2+\Gamma^2+2\Gamma\Psi(t)\ \text{ for }\ \Psi\ll\Gamma,\end{aligned}\tag{8}$$

with σ^2 the polarizer extinction ratio and Γ the total static ellipticity. This static ellipticity is due to the mirrors' intrinsic phase retardation [14]. Each mirror can be regarded as a wave plate. The combination of both wave plates gives a single wave plate with a total phase retardation and an axis orientation that depend on each mirror phase retardation and on their relative orientation [15,16]. Thus, we adjust the value of Γ by rotating the mirrors M_1 and M_2 around the z axis corresponding to the axis of light propagation.

To measure the polarizer extinction ratio, we first set $\Gamma=0$, with no magnetic field. We get $I_{\rm e}/I_{\rm t,f}=\sigma^2\sim7\times10^{-7}$. Then, to reach the best sensitivity, we need $\Gamma^2\sim\sigma^2$ [9]. Starting from $\Gamma=0$ and rotating M_1 in the clockwise or counterclockwise direction, we choose the value of Γ as well as its sign determined by CM measurements in nitrogen and helium gas. The measurement of σ^2 and the adjustment of the value and sign of Γ are done before each magnetic pulse.

Due to the photon lifetime, the cavity acts as a first order low pass filter, as explained in details in Ref. [17]. Its complex response function $H(\nu)$ is given by :

$$H(\nu)=\frac{1}{1+i\frac{\nu}{\nu_{\rm c}}},\tag{9}$$

with ν the frequency and $\nu_{\rm c}=1/4\pi\tau\simeq74\,\rm Hz$ the cavity cutoff frequency. This filtering has to be taken into account in particular for the time dependent magnetic field applied inside the Fabry-Pérot cavity. The ellipticity Ψ induced by the external magnetic field is thus proportional to $B_{\rm f}^2$:

$$\Psi(t)=\alpha B_{\rm f}^2(t),\tag{10}$$

where the filtered field $B_{\rm f}^2$ is calculated from B^2 taking into account the cavity filtering. The time profile of $B_{\rm f}^2$ is plotted in Fig. 3 with the dashed curve. In particular, the cavity filtering induces an attenuation and a shift of the maximum. The cavity filtering has also to be applied to $I_{\rm t}$ as explained in details in Refs. [17,11].

The calculated signals used for the analysis are described in details in Ref. [11]. In order to extract the ellipticity $\Psi(t)$ from Eq. (8), we calculate the following $Y(t)$ signal after each pulse :

$$Y(t)=\frac{\frac{I_{\rm e}(t)}{I_{\rm t,f}(t)}-I_{\rm dc}}{2\mid\Gamma\mid},\tag{11}$$

$$\simeq\gamma\Psi(t),\tag{12}$$

where γ corresponds to the sign of Γ. We calculate the static signal $I_{\rm dc}=\sigma^2+\Gamma^2$ before the pulse as follows :

$$I_{\rm dc}=\left\langle\frac{I_{\rm e}(t)}{I_{\rm t,f}(t)}\right\rangle\Big|_{t_\Gamma<t<0},\tag{13}$$

where t_Γ corresponds to the beginning of the analysis and $t=0$ to the beginning of the applied magnetic field. The absolute value of the cavity ellipticity is measured a few milliseconds before each magnetic pulse thanks to the following equation :

$$|\Gamma|=\sqrt{\left\langle\frac{I_{\rm e}(t)}{I_{\rm t,f}(t)}\right\rangle\Big|_{t_\Gamma<t<0}-\sigma^2}.\tag{14}$$

Signals $Y(t)$ are collected for both signs of Γ and for both directions of $\boldsymbol{B}$: parallel to x is denoted as >0 and antiparallel is denoted as <0. This gives four data series : ($\Gamma>0$, $B>0$), ($\Gamma>0$, $B<0$), ($\Gamma<0$, $B<0$) and ($\Gamma<0$, $B>0$). For each series, signals calculated with Eq. (11) are averaged and denoted as $Y_{>>}$, $Y_{><}$, $Y_{<<}$ and $Y_{<>}$. The first subscript corresponds to $\Gamma>0$ or <0 and the second one corresponds to $\boldsymbol{B}$ parallel or antiparallel to x.

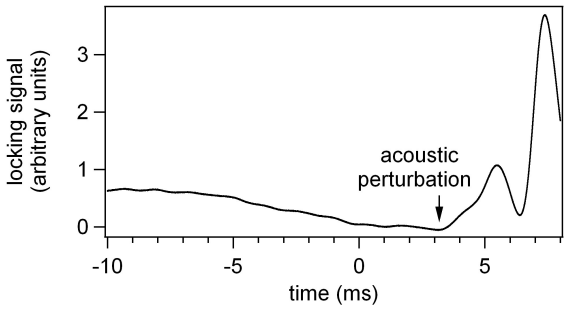

Figure 4. Time evolution of the locking signal during a magnetic pulse. The magnetic field is applied at $t = 0$ ms.

3 Data analysis and results

The raw signals, such as $I_{\rm t}(t)$, $I_{\rm e}(t)$, $B(t)$ or the cavity locking signal, are recorded 25 ms before the beginning of the magnetic field and 25 ms after. A typical cavity locking signal is plotted in Fig. 4. We clearly see a perturbation which begins at about 3.2 ms. This corresponds to the acoustic perturbation triggered at $t = 0$ by the magnetic pulse. This perturbation travels trough the air to the mirror mounts. We have confirmed the arrival time on the mirror mounts with accelerometers. This perturbation induces an ellipticity noise which degrades our sensitivity. We have thus decided to stop the analysis at $t = 3.1$ ms. Symmetrically, we start the analysis at $t_\Gamma = -3.1$ ms. It also allows to avoid drifts and long time variations of Γ.

For each pulse applied in vacuum, we first calculate the $|\Gamma|$ value following Eq. (14). To check that this corresponds to a meaningful value, we plot the histogram of the following signal for $t_\Gamma < t < 0$:

$$\Psi(t) = \sqrt{\frac{I_{\rm e}(t)}{I_{\rm t,f}(t)} - \sigma^2} - \Gamma. \qquad (15)$$

This corresponds to 3100 values acquired every 1 μs. With white noise and because no induced ellipticity is present at $t < 0$, the histogram is centered on 0 and corresponds to a gaussian distribution, as shown in Fig. 5a.

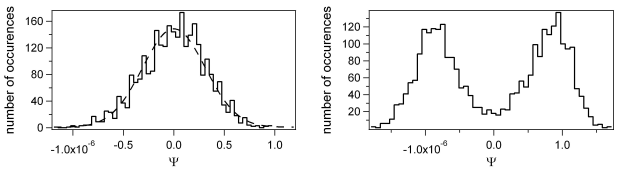

(a) (b)

Figure 5. Typical histogram of $\Psi(t)$ before the magnetic pulse. a) The histogram can be fitted by a gaussian function (dashed curve) : the shot is selected. b) Rejected shot.

However, some of the histograms cannot be fitted by a gaussian function, as shown in Fig. 5b. The main origin of this type of distributions is mechanical oscillations of the setup induced by the environment and leading to static ellipticity fluctuations, event if the magnetic filed is not applied. These mechanical oscillations can be directly observed on the power spectral density (PSD) of the ellipticity Ψ in the absence of the magnetic field, as shown in Fig. 6. In the case corresponding to Fig. 5b, we cannot give a statistical and significant value of Γ. The corresponding shots are thus rejected. Finally we selected 101 pulses. It should be noted that this selection is performed for $t < 0$, thus before the magnetic pulse. We do not select or reject pulses with an analysis on the signal we want to measure, thus induced by the magnetic field at $t > 0$.

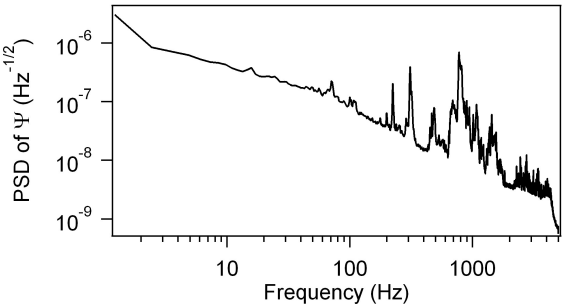

Figure 6. Power spectral density of Ψ in the absence of the magnetic field. We observe the different mechanical resonances of the setup.

From the 101 selected pulses, we calculate the signals $Y_{>>}$, $Y_{><}$, $Y_{<<}$, and $Y_{<>}$, denoted by $Y_{\rm j}$ with j =>>, >< , >>, <>. As explained in section 2.2, they correspond to the average of the $Y(t)$ signals calculated with Eq. (11) for each of the four series. The $Y_{\rm j}$ uncertainties are calculated at each time $t_{\rm i}$, $\Delta Y_{\rm j}(t_{\rm i}) = \sigma_{\rm j}(t_{\rm i})/\sqrt{N_{\rm j}}$, with $\sigma_{\rm j}(t_{\rm i})$ the standard deviation of the $Y_{\rm j}(t_{\rm i})$ distribution and $N_{\rm j}$ the number of shots for the j series.

As explained in details in Ref. [11], one has to consider systematic effects that mimic the CM effect we want to measure. We thus analyze our data following a general expression taking into account the symmetry properties of $Y_{\rm j}$ towards experimental parameters :

$$\begin{aligned}
Y_{>>} &= a_{>>}S_{++} + b_{>>}S_{+-} + c_{>>}S_{--} + d_{>>}S_{-+},\\
&= a_{>>}S_{++} + b_{>>}S_{+-} + c_{>>}S_{--} + \Psi,\\
Y_{><} &= a_{><}S_{++} - b_{><}S_{+-} - c_{><}S_{--} + d_{><}S_{-+},\\
&= a_{><}S_{++} - b_{><}S_{+-} - c_{><}S_{--} + \Psi,\\
Y_{<<} &= a_{<<}S_{++} - b_{<<}S_{+-} + c_{<<}S_{--} - d_{<<}S_{-+},\\
&= a_{<<}S_{++} - b_{<<}S_{+-} + c_{<<}S_{--} - \Psi,\\
Y_{<>} &= a_{<>}S_{++} + b_{<>}S_{+-} - c_{<>}S_{--} - d_{<>}S_{-+},\\
&= a_{<>}S_{++} + b_{<>}S_{+-} - c_{<>}S_{--} - \Psi.
\end{aligned}$$

The S functions correspond to a given symmetry towards the sign of Γ and the direction of $\boldsymbol{B}$. The first subscript +

(resp. −) indicates an even (resp. odd) parity with respect to the sign of Γ. The same convention is used for the second subscript corresponding to $\boldsymbol{B}$. Each S function has a different physical origin which are summarized in Tab. 1. CM effect signal contributes to S_{-+} since it depends on the cavity birefringence Γ and on the square of the magnetic field amplitude as shown in Eqs. (5) and (12). We can thus replace dS_{-+} by $\gamma\Psi$.

S signal	Physical effect
$S_{++}(t)$	$\Theta_{\rm F}^2(t)$, $\Psi^2(t)$
$S_{+-}(t)$	$\boldsymbol{B}$ effects on photodiodes
$S_{--}(t)$	$\gamma\Theta_{\rm F}(t)$
$S_{-+}(t)$	$\gamma\Psi(t)$

Table 1. Possible physical effects contributing to the S signals. The $\Theta_{\rm F}$ signal corresponds to a polarization rotation angle due to the circular birefringence induced by a longitudinal magnetic field (Faraday effect).

The S functions are then extracted with a linear combination of $Y_{\rm j}$ as follows :

$$\begin{aligned}
J_1 &\equiv \frac{Y_{>>}+Y_{><}+Y_{<<}+Y_{<>}}{4},\\
&= \overline{a}\ S_{++} + \Delta b_1\ S_{+-} + \Delta c_1\ S_{--} + \Delta d_1\ S_{-+},\\
J_2 &\equiv \frac{Y_{>>}-Y_{><}-Y_{<<}+Y_{<>}}{4},\\
&= \Delta a_2\ S_{++} + \overline{b}\ S_{+-} + \Delta c_2\ S_{--} + \Delta d_2\ S_{-+},\\
J_3 &\equiv \frac{Y_{>>}-Y_{><}+Y_{<<}-Y_{<>}}{4},\\
&= \Delta a_3\ S_{++} + \Delta b_3\ S_{+-} + \overline{c}\ S_{--} + \Delta d_3\ S_{-+},\\
J_4 &\equiv \frac{Y_{>>}+Y_{><}-Y_{<<}-Y_{<>}}{4},\\
&= \Delta a_4\ S_{++} + \Delta b_4\ S_{+-} + \Delta c_4\ S_{--} + \overline{d}\ S_{-+}.
\end{aligned} \tag{16}$$

$J_1(t)$, $J_2(t)$, $J_3(t)$ and $J_4(t)$ are plotted in Fig. 7. Their uncertainties are calculated from the $Y_{\rm j}$ uncertainties. The weighting parameters a, b, c and d depend on the experimental adjustment from pulse to pulse and from day to day. Their relative variations are small : $\Delta a/\overline{a}$, $\Delta b/\overline{b}$, $\Delta c/\overline{c}$, $\Delta d/\overline{d} \ll 1$. Δa, Δb and Δc are mainly due to the Γ variation from one shot to another and we can precisely calculate them since Γ is measured for each shot. We obtain $\Delta a_4/\overline{a} = 5.97\times10^{-2}$, $\Delta b_4/\overline{b} = -7.67\times10^{-2}$ and $\Delta c_4/\overline{c} = -8.27\times10^{-2}$. These values are of the same order of magnitude as the one obtained during the CM measurement of helium gaz [11]. Δd is independent of the Γ variation. It mainly comes from a variation of the magnetic field from one pulse to another. As the B relative variation is small compared to the Γ relative variation we consider $\Delta d \simeq 0$. The variation of Ψ is thus neglected.

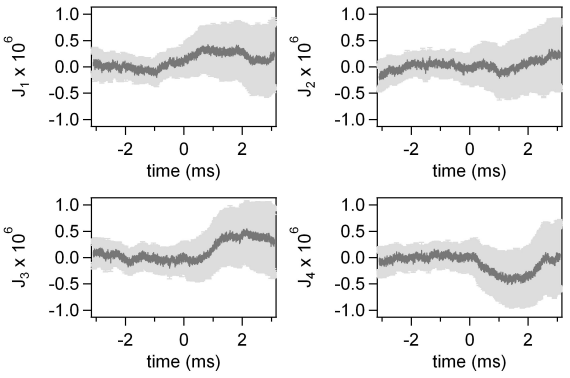

Figure 7. Time evolution of J_1, J_2, J_3 and J_4 (dark grey curve) and their uncertainties at 3σ confidence level (light grey).

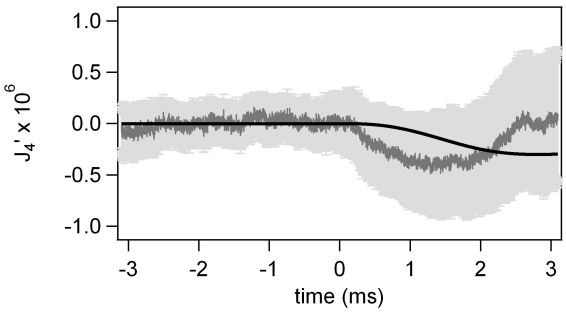

Figure 8. Dark grey curve : time evolution of J_4' and its 3σ uncertainties (light grey). Black curve : $\alpha B_{\rm f}^2$ function superimposed to guide the eyes.

We thus write :

$$\begin{aligned}
J_1 &\simeq \overline{a}\ S_{++},\\
J_2 &\simeq \overline{b}\ S_{+-},\\
J_3 &\simeq \overline{c}\ S_{--},\\
J_4 &\simeq \frac{\Delta a_4}{\overline{a}}J_1 + \frac{\Delta b_4}{\overline{b}}J_2 + \frac{\Delta c_4}{\overline{c}}J_3 + \Psi.
\end{aligned} \tag{17}$$

We then calculate :

$$\begin{aligned}
J_4' &\equiv J_4 - \left[\frac{\Delta a_4}{\overline{a}}J_1 + \frac{\Delta b_4}{\overline{b}}J_2 + \frac{\Delta c_4}{\overline{c}}J_3\right],\\
&\simeq \Psi,
\end{aligned} \tag{18}$$

which corresponds to the Cotton-Mouton signal. It is plotted in Fig. 8 together with a $\alpha B_{\rm f}^2$ function superimposed to guide the eyes. Nevertheless, we see that the major component of J_4' is not $\alpha B_{\rm f}^2$ but a supplementary systematic effect.

As sais before, the setup is subject to several mechanical resonances which can be excited both by the environment and the magnetic field. The latter could thus trigger a mechanical oscillation of the setup at $t = 0$. We try to fit J_4' by a sine function starting at $t = 0$. The fit gives a frequency of (180 ± 3) Hz and it is superimposed

to J_4' in Fig. 9a. We finally fit the residues by $\alpha B_{\rm f}^2$. The fit is superimposed to the residues of J_4' in Fig. 9b. The Cotton-Mouton constant $k_{\rm CM}$ is deduced from the measured experimental parameters as follows [10] :

$$k_{\rm CM} = \frac{\alpha}{4\pi\tau\Delta^{\rm FSR}}\frac{\lambda}{L_B}\frac{1}{\sin 2\theta_{\rm P}}. \qquad (19)$$

We obtain :

$$k_{\rm CM} = (-0.9 \pm 6.2) \times 10^{-21}\,{\rm T}^{-2}, \qquad (20)$$

at 3σ confidence level. As said before we give error bars at 3σ corresponding to a confidence level of 99.8%, that usually indicates an evidence for a non-zero signal. The uncertainty takes into account the A-type and B-type uncertainties. The A-type uncertainties come from the fit and from the photon lifetime with a relative variation lower than 6% at 3σ. The B-type uncertainties have been evaluated previously and detailed in Ref. [10]. They essentially come from the length of the magnetic field L_B with a relative uncertainty of 6.6% at 3σ. The value of Eq. (20) gives an estimate of our noise floor, which is half the one of the PVLAS collaboration in 2012 obtained with an integration time of 8192 s [8].

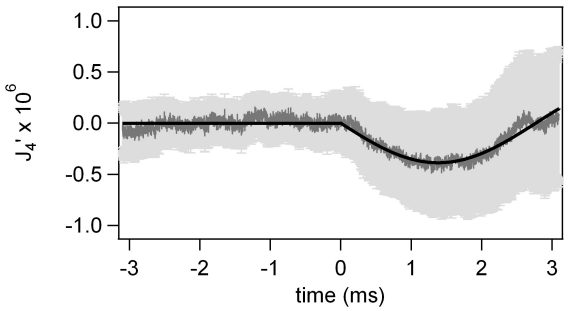

(a) Time evolution of J_4'. Black curve : fit with a sine function at 180 Hz.

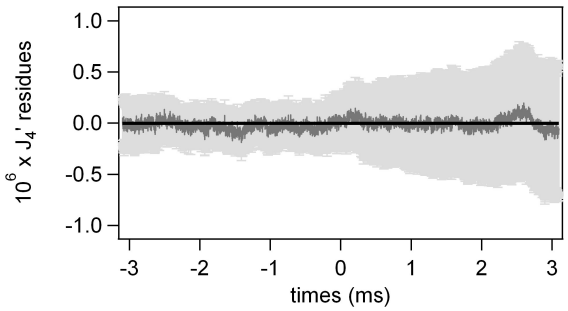

(b) Time evolution of the residues of J_4'. Black curve : fit with $\alpha B_{\rm f}^2$.

Figure 9. Time evolution of J_4' and its residues (dark grey). The 3σ uncertainties are superimposed in light grey.

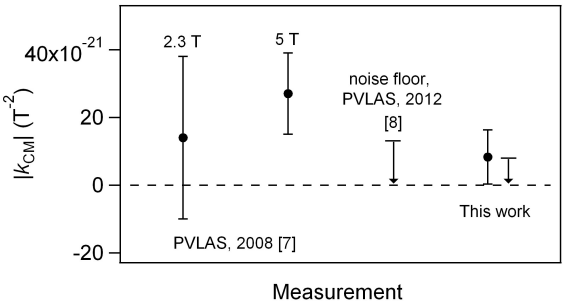

Figure 10. Comparison of the latest absolute reported values of the vacuum CM effect. Error bars are given at 3σ. This work : black dot, value obtain with the fit combining the sine function at 177 Hz and the $\alpha B_{\rm f}^2$ function ; arrow, noise floor of $8.0 \times 10^{-21}\,{\rm T}^{-2}$.

In order to assess more precisely the physical origin of the systematic effect, we zoom in the power spectral density of Ψ, depicted in Fig. 6, on the frequencies around 180 Hz. We find several resonances at 177 Hz, 200 Hz and above. The signal J_4' is then fitted by a sine function but with the frequency fixed to each of the resonance frequencies. The best fit, corresponding to the best χ^2, is obtained for 177 Hz, which is compatible with the frequency given by the previous fit. Fitting the residues by $\alpha B_{\rm f}^2$ gives our final value for the CM constant :

$$k_{\rm CM} = (5.1 \pm 6.2) \times 10^{-21}\,{\rm T}^{-2}, \qquad (21)$$

at 3σ confidence level.

On the other hand, if we fit the data corresponding to Fig. 8 with the sum of the sine function of 177 Hz frequency and $\alpha B_{\rm f}^2$, we obtain :

$$k_{\rm CM} = (8.3 \pm 8.0) \times 10^{-21}\,{\rm T}^{-2}, \qquad (22)$$

at 3σ confidence level.

All this shows that our noise floor given by the uncertainties is of a few $10^{-21}\,{\rm T}^{-2}$ while the central value depends on the fitting procedure. Establishing what is the most statistically appropriate fitting procedure is out of the scope of this paper. Our goal is to report on our noise floor and to highlight the main contributions to systematic effects in order to improve the overall sensitivity of the next version of the apparatus.

Nevertheless, for the sake of comparison we show in Fig. 10 our typical value given in Eq. (22) together with the already published values. We see that our value is slightly better than the previous one.

4 Conclusions and perspectives

We presented the last advances of our BMV apparatus in terms of the best noise floor of vacuum magnetic birefringence ever realized. Our result validates our experimental method based on pulsed fields. In particular, it proves that the sensitivity obtained in a single pulse

compensates the loss of duty cycle. To reach the QED value, the needed improvement is of three orders of magnitude. This is not conceivable with this first-generation experiment. Our strategy is therefore to increase the magnetic field thanks to the pulsed technology. At the moment, we have $B^2L_B = 5.8\,\mathrm{T}^2\mathrm{m}$ but we conceptualized and tested a pulsed coil that has already reached a B^2L_B higher than $300\,\mathrm{T}^2\mathrm{m}$. Two coils of this type will be inserted in the experiment in the near future. This essential step really makes the vacuum birefringence measurement within our reach.

On the other hand, our analysis has allowed us to identify some systematic effects. Obviously, a special care will be devoted to limit them in order to improve the accuracy. The magnetic field induces an excitation on the setup which resonates at different frequencies. Since it affects the signal J_4, the resonance at 177 Hz has an odd symmetry with respect to the sign of Γ. This implies that it concerns the mirror mounts. In order to get rid of this effect, a new setup was designed, providing a better magnetic insulation of the mirrors. It will also provide a better acoustic insulation of the mirror mounts, improving the overall sensitivity and decreasing the number of rejected shots. Moreover in the new version of our setup we will be able to measure the ellipticity both with θ_P equal to 0° (no induced ellipticity) and 45° (maximal induced ellipticity). This will allow us to subtract from the raw data the systematic effects that do not depend on the polarization direction, as the sine function at 177 Hz.

5 Acknowledgments

We thank all the members of the BMV collaboration, and in particular J. Béard, J. Billette, P. Frings, B. Griffe, J. Mauchain, M. Nardone, J.-P. Nicolin and G. Rikken for strong support. We are also indebted to the whole technical staff of LNCMI. We acknowledge the support of the *Fondation pour la recherche IXCORE* and the ANR-Programme non Thématique (Grant No. ANR-BLAN06-3-139634).

Références

1. C. Rizzo, A. Rizzo and D. M. Bishop, Int. Rev. Phys. Chem. **16**, 81 (1997).
2. Z. Bialynicka-Birula and I. Bialynicki-Birula, Phys. Rev. D **2**, 2341 (1970).
3. V. I. Ritus, Sov. Phys. JETP **42**, 774 (1975).
4. R. Battesti and C. Rizzo, Rep. Prog. Phys. **76**, 016401 (2013).
5. P. J. Mohr, B. N. Taylor, and D. B. Newell, Rev. Mod. Phys. **84**, 1527 (2012).
6. R. Cameron, G. Cantatore, A. C. Melissinos, G. Ruoso, Y. Semertzidis, H. J. Halama, D. M. Lazarus, A. G. Prodell, F. Nezrick, C. Rizzo and E. Zavattini, Phys. Rev. D **47**, 3707 (1993).
7. E. Zavattini, G. Zavattini, G. Ruoso, G. Raiteri, E. Polacco, E. Milotti, V. Lozza, M. Karuza, U. Gastaldi, G. Di Domenico, F. Della Valle, R. Cimino, S. Carusotto, G. Cantatore and M. Bregant, Phys. Rev. D **77**, 032006 (2008).
8. G. Zavattini, U. Gastaldi, R. Pengo, G. Ruoso, F. Della Valle and E. Milotti, Int. J. of Mod. Phys. A **27**, 1260017 (2012).
9. R. Battesti, B. Pinto Da Souza, S. Batut, C. Robilliard, G. Bailly, C. Michel, M. Nardone, L. Pinard, O. Portugall, G. Trénec, J.-M. Mackowski, G. L. J. A. Rikken, J. Vigué and C. Rizzo, Eur. Phys. J. D **46**, 323 (2008).
10. P. Berceau, M. Fouché, R. Battesti and C. Rizzo, Phys. Rev. A **85**, 013837 (2012).
11. A. Cadène, D. Sordes, P. Berceau, M. Fouché, R. Battesti and C. Rizzo, Phys. Rev. A **88**, 043815 (2013).
12. R. W. P. Drever, J. L. Hall, F. V. Kowalski, J. Hough, G. M. Ford, A. J. Munley and H. Ward, Appl. Phys. B **31**, 97 (1983).
13. S. Batut, J. Mauchain, R. Battesti, C. Robilliard, M. Fouché and O. Portugall, IEEE Trans. Applied Supercond. **18**, 600 (2008).
14. F. Bielsa, A. Dupays, M. Fouché, R. Battesti, C. Robilliard and C. Rizzo, Appl. Phys. B **97**, 457 (2009).
15. D. Jacob, M. Vallet, F. Bretenaker, A. Le Floch and M. Oger, Opt. Lett. **20**, 671 (1995).
16. F. Brandi, F. Della Valle, A.M. De Riva, P. Micossi, F. Perrone, C. Rizzo, G. Ruoso and G. Zavattini, Appl. Phys. B **65**, 351 (1997).
17. P. Berceau, M. Fouché, R. Battesti, F. Bielsa, J. Mauchain and C. Rizzo, Appl. Phys. B **100**, 803 (2010).
18. G. Bialolenker, E. Polacco, C. Rizzo and G. Ruoso, Appl. Phys. B **68**, 703 (1999).